NANO LETTERS

Letter

pubs.acs.org/NanoLett

Porous Amorphous $FePO_4$ Nanoparticles Connected by Single-Wall Carbon Nanotubes for Sodium Ion Battery Cathodes

Yonglin Liu,[†,§] Yunhua Xu,[‡,§] Xiaogang Han,[†] Chris Pellegrinelli,[†] Yujie Zhu,[‡] Hongli Zhu,[†] Jiayu Wan,[†] Alex Chong Chung,[†] Oeyvind Vaaland,[†] Chunsheng Wang,*[,‡] and Liangbing Hu*[,†]

[†]Department of Materials Science and Engineering, University of Maryland, College Park, Maryland 20742, United States

[‡]Department of Chemical Engineering, University of Maryland, College Park, Maryland 20742, United States

Supporting Information

ABSTRACT: Sodium ion batteries (SIBs) are promising candidates for the applications of large-scale energy storage due to their cost-effective and environmental-friendly characteristics. Nevertheless, it remains a practical challenge to find a cathode material of SIBs showing ideal performance (capacity, reversibility, etc.). We report here a nanocomposite material of amorphous, porous $FePO_4$ nanoparticles electrically wired by single-wall carbon nanotubes as a potential cathode material for SIBs. The hydrothermally synthesized nanocomposite shows excellent cell performance with unprecedented cycling stability and reversibility. The discharge capacity of as high as 120 mAh/g is delivered at a 0.1 C rate (10 mA/g). The capacity retentions are about 70 mAh/g, 60 mAh/g, and 55 mAh/g at higher currents of 20 mA/g, 40 mA/g, and 60 mA/g, respectively. Even at a 1 C rate (100 mA/g), a capacity of about 50 mAh/g is still retained after 300 cycles. With a simple synthetic procedure, cost-effective chemicals, and desirable cell performance, this method offers a highly promising candidate for commercialized cathode materials of SIBs.

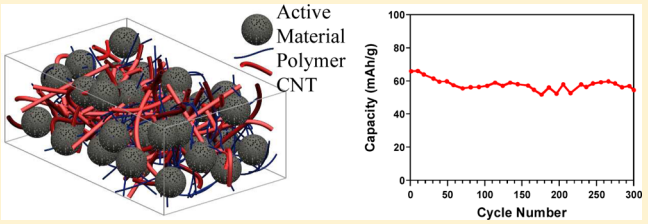

KEYWORDS: *Grid energy storage, Na-ion battery, cathodes material, amorphous $FePO_4$*

Recently, sodium ion batteries (SIBs) have drawn increasing attention from researchers, despite the fact that lithium ion batteries (LIBs) are still the predominant power source for home electronics and for future large-scale energy storage devices.[1−4] Compared with LIBs, SIBs can be manufactured using more abundant resources, far lower prices, and a greener synthesis while maintaining a similarity in ion insertion chemistry.[1−4] However, many challenges remain before SIBs can become commercially competitive with LIBs. For instance, compared to lithium, sodium weighs more and has a higher ionization potential[3] and a larger ionic radius.[5] Further, recent computational studies show that the voltages for the intercalation materials are 0.18−0.57 V lower than that of the corresponding Li voltages.[1] The smaller energy density of SIBs as compared to LIBs can nevertheless be compensated by the earth-abundance and lower cost of Na, thus making SIBs more promising candidates for commercialized large-scale energy devices and stationary storage.[2]

Since the characteristic performance of SIBs including specific capacity and operation voltage is largely dependent on the electrochemical properties of the electrode materials, it is of great importance to develop suitable electrode materials for SIBs. A few examples of cathode materials were developed and tested for SIBs.[1−4,6] Among them, iron phosphate-based materials show great potential as environmentally friendly and cost-effective cathodes for SIBs due to their thermal stability and higher voltage.[3] There exist two crystalline phases for sodium iron phosphate ($NaFePO_4$), the maricite phase and the olivine phase.[6] The olivine $NaFePO_4$ is the electrochemically active phase showing a very similar channel structure to its Li counterpart. As the thermally stable phase, the maricite $NaFePO_4$ shows a structure of one-dimensional, edge-sharing FeO_6 octahedrons in the absence of any cationic channel, thus appearing to be electrochemically inactive. Consequently, a direct chemical synthesis pathway appears to be unsuccessful for the olivine $NaFePO_4$, which, currently, can only be produced through the cation exchange method from $LiFePO_4$.[6,7] This makes crystalline $NaFePO_4$ a less appealing substitute for the matching LIBs. It is thus of great significance to develop a noncrystalline iron phosphate cathode material through direct chemical synthesis. Amorphous $FePO_4$ nanostructures, which have been previously investigated for the Li ion battery,[8,9] are promising candidates for SIBs. Compared with crystalline $FePO_4$ materials, amorphous $FePO_4$ shows the advantages of a simple and low temperature synthetic procedure, as well as providing reliable continuous pathways for metal ions (Na^+ or Li^+) during the charge−discharge process.

The vast majority of previous research regarding $FePO_4$-related cathode materials of SIBs has demonstrated much poorer cell performance. For instance, Zaghib et al. showed that

Received: July 30, 2012
Revised: September 24, 2012
Published: October 16, 2012

the crystalline $NaFePO_4$ material produced from an electrochemical pathway can have a specific capacity of 147 mA h g^{-1}, however performing poorly in reversibility with a capacity of 50.6 mA h g^{-1} in the second cycle.[10] As other previous research disclosed less complete results in terms of performance (reversibility, stability, etc.),[4,6] it is necessary to revisit the same cathode material for SIBs with an emphasis of performance.

Amorphous $FePO_4$ materials are, however, considered as a conceptual defect-free phase. Defect-insensitive behaviors of Li ion have been demonstrated with amorphous $FePO_4$ as a cathode material for the Li-ion battery. Previous reports show that amorphous $FePO_4$ nanoparticles of 10−20 nm, produced from engineered virus structures[9] or graphene hybrids,[11] show a first discharge capacity of 165 (at 0.1 C) and 140 mA h g^{-1} (at 0.125 C), respectively, when used as cathode materials for Li-ion batteries. The theoretical capacity of this nanostructured material is as high as 178 mA h g^{-1}.[12] To the best of our knowledge, similar nanostructures have not previously been applied in the field of Na-ion batteries. In the present work, we apply a simple hydrothermal method to produce a networked nanocomposite of single-wall carbon nanotubes (SWNTs)/amorphous porous $FePO_4$ nanoparticles for SIBs (Figure 1).

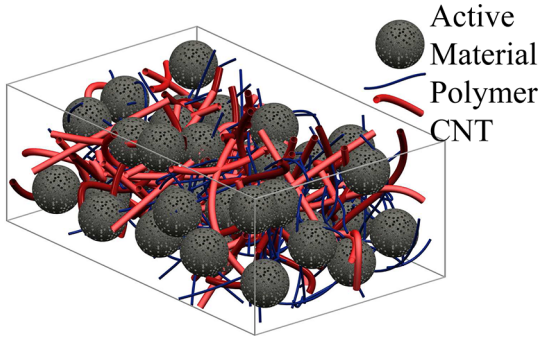

Figure 1. Systematic diagram for the nanocomposite of SWNT−amorphous porous $FePO_4$ nanoparticles.

The porous structures of the amorphous $FePO_4$ will provide further assistance for Na^+ migration, which appears to be much larger than Li^+. The interconnecting SWNTs will provide conductive pathways for electron transportation.

The synthesis follows a one-step hydrothermal approach, and a similar protocol of graphene−amorphous $FePO_4$ hollow nanosphere hybrids has been reported previously.[11] In a typical synthesis, iron(II) ammonium sulfate ($(NH_4)_2Fe(SO_4)_2$, 0.0392 g), phosphoric acid (H_3PO_4, 41 μL), urea (1.2 g), and sodium dodecylsulfate (SDS, 0.1 g), along with 20 mg of SWNTs (−COOH or −OH functionalized), were dissolved in 20 mL of DI-water. The mixture was then vigorously stirred for 5−10 min, transferred into an autoclave, and heated to maintained temperature of 80 °C, which was maintained for 12 h. The resulting products were collected by centrifugation and washed subsequently with anhydrous ethanol and DI-water three times. The final products were obtained after drying at 80 °C for 12 h.

The transmission electron microscopic (TEM) images (Figure 2a) indicate that the as-prepared $FePO_4$ nanoparticles (NPs), with a size range of 30−300 nm, are interconnecting with SWNTs, forming a closely interacted network of nanocomposites. High-resolution TEM images clearly illustrate the porous (Figure 2b) and amorphous (Figure 2c) nature of these $FePO_4$ NPs. The inner cavities are clearly revealed by the contrast between the inner and outer part of the spheres (Figure 2b). The sizes of the porous space within $FePO_4$ NPs range from a few to tens of nanometers. The scanning electron microscopy (SEM) images (Figure 3a) further confirm the interconnecting network of SWNTs and amorphous $FePO_4$ NPs. The energy dispersive X-ray spectroscopy (EDX) mapping analysis shows that the nanoparticles are composed of Fe, P, and O, confirming the composition (Figure 3b).

As shown in Figure S1 in the Supporting Information, the porous nature of the surfaces of the $FePO_4$ nanoparticles is clearly visualized, and the size of the cavities is in the range of 1−10 nm. This observation is further confirmed with our Brunauer−Emmett−Teller (BET) surface analysis on the $FePO_4$ nanoparticles. As shown in Figure S4 in the Supporting Information, the surface area and pore size of the $FePO_4$ nanoparticles were tested with a Micromeritics ASAP 2020 Porosimeter Test Station. The testing range of pore size is between 17.000 Å and 3000.000 Å. The BET surface area is determined to be 222.5351 m^2/g, and the Barrett−Joyner−Halenda (BJH) adsorption average pore width (4 V/A) is 97.673 Å. On the basis of the N_2 adsorption/desorption isotherm distribution plot, we can derive that most of the pores areis distributed in the nanometer range. Further, Figure S2 in the Supporting Information includes additional SEM images of the as-prepared complex of the FePO4 nanoparticles and SWNTs, showing the interconnecting network nature of the complex. As shown in Figure S2, the spherical-shaped $FePO_4$ nanoparticles (marked with blue arrows) are indisputably connected by SWNTs/or their bundles (marked with red arrows), forming an interconnecting network of the complex. Further, Figure S3 includes additional TEM images of the as-prepared complex of the $FePO_4$ nanoparticles and SWNTs, showing both the amorphous and porous nature of the $FePO_4$ nanoparticles and the interconnecting network nature of the complex. As shown in Figure S3, the amorphous and porous nature of the $FePO_4$ nanoparticles is confirmed by the contrast in the images, and note that the same strategies have been used to determine porous or hollow interior structures by quite a few groups.[8,15] Moreover, on the basis of a comparison between our observations and the previous reported data,[8,15] we believe that the porous structures of cavities not only exist on the surface of the $FePO_4$ nanoparticles as shown in the above SEM images, but also in the interiors of the nanoparticles, indicated by TEM images (Figure S3) and BET data (Figure S4). The interconnecting nature of the $FePO_4$ nanoparticles and SWNTs is also confirmed by Figure S3. To further confirm the amorphous nature of the $FePO_4$ nanoparticles in the complex, X-ray diffraction (XRD) study has been performed. The XRD spectroscopy of the as-prepared complex of the $FePO_4$ nanoparticles and SWNTs is shown in Figure S5. The two broad peaks observed at 25 and 44 are corresponding to SWNTs, in good agreement with a previous report.[8] The absence of the characteristic peaks of the corresponding crystalline $FePO_4$, along with the energy dispersive X-ray spectroscopy (EDX) mapping analysis showing that the nanoparticles are composed of $FePO_4$ (Figure 3b), indicates the amorphous nature of the $FePO_4$ nanoparticles.

The as-prepared network of SWNTs and amorphous $FePO_4$ NPs are promising cathode materials for SIBs. Na ions can easily diffuse in and out of the amorphous $FePO_4$ NPs due to their periodic, porous structures at the nanometer scale. The interconnecting SWNTs provide fast transport pathways for

dx.doi.org/10.1021/nl302819f | Nano Lett. 2012, 12, 5664−5668

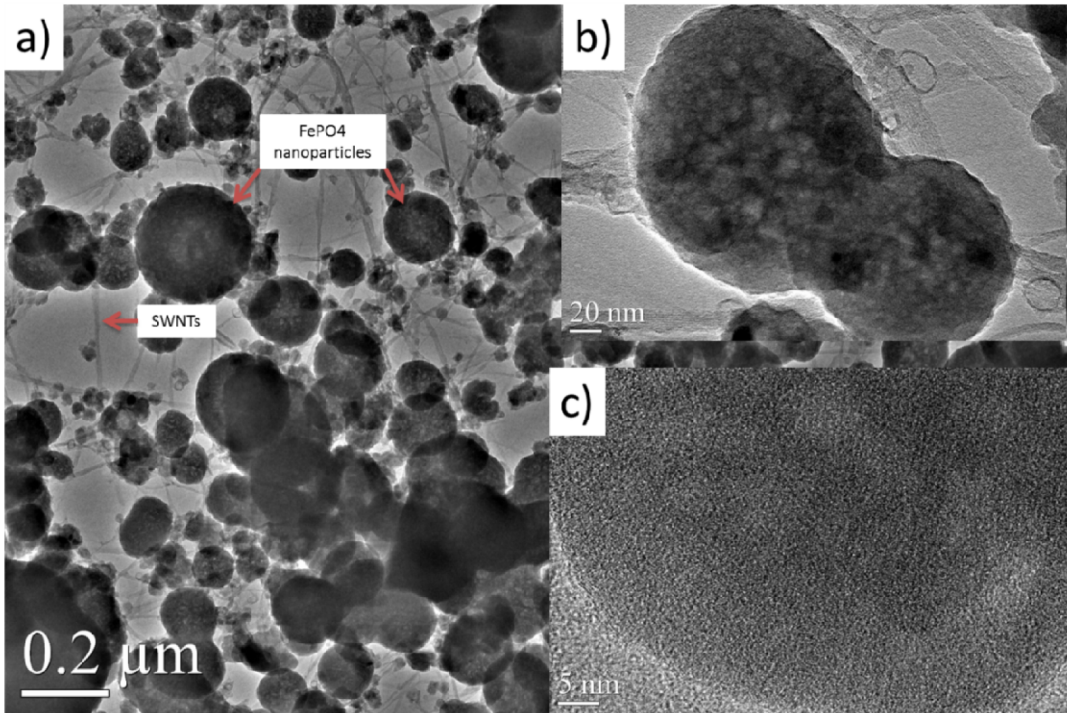

Figure 2. (a) TEM images of the as-prepared networks of SWNTs-amorphous porous $FePO_4$ nanoparticles. High-resolution images of (b) two $FePO_4$ nanoparticles on SWNTs and (c) one individual nanoparticle, showing the amorphous nature.

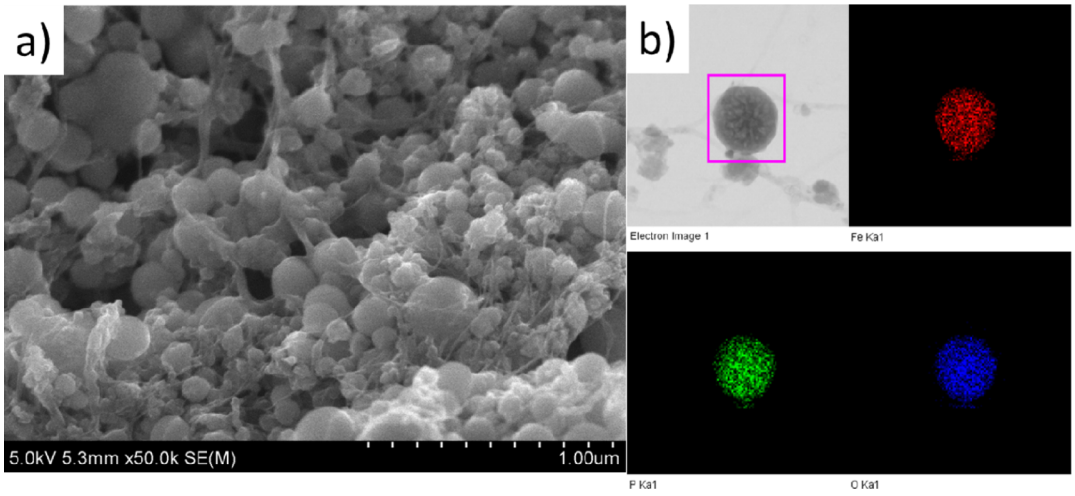

Figure 3. (a) SEM images of the as-prepared nanocomposites, showing interconnecting amorphous $FePO_4$ nanoparticle with SWNTs. (b) Elemental mapping analysis of the one individual $FePO_4$ nanoparticle, showing the compositions of Fe (red), P (green), and O (blue).

electrons, which provides effective transport between the individual porous $FePO_4$ NPs. Thus, these nanocomposite materials are expected to significantly enhance battery performance by improving Na ion and electron transport. Moreover, the rough surfaces of the $FePO_4$ NPs provide more interface area between the active materials ($FePO_4$) and the electrolyte. In the present synthetic procedure, multiwall carbon nanotubes or graphene, which have a much lower cost compared to SWNTs, can be used to produce the corresponding nanocomposites of amorphous FePO4 and carbon-based materials.

The electrochemical performance of the $FePO_4$/SWNTs composite was examined in a coin cell using sodium as the counter electrode. Figure 4a shows the charge/discharge profiles in the 10th, 100th, 200th, and 300th cycles of the amorphous $FePO_4$/SWNTs composite. Different from crystalline materials, whose potential plateaus are a typical feature due to phase transitions caused by ion insertion/extraction,[6,13] smooth slopes were observed with the evolution of sodium ion insertion/extraction in our material. This confirms the amorphous structure of the porous $FePO_4$ in the composite. Based on the studies of porous materials for Li-ion cells,[8,14,15] it could be suggested that sodium ions were inserted in or adhered to the surface of porous $FePO_4$, which is superior to what is seen for bulk materials. Figure 4b and c shows the cycling stability and Coulombic efficiency at a current density of 50 mA/g. The $FePO_4$/SWNT composite delivered charge and discharge capacities of as high as 98 mAh/g and 66 mAh/g, respectively, in the first cycle, corresponding to a Coulombic efficiency of 67%. The capacity slightly decreased to ~60 mAh/g and then became stable up to 300 cycles. The Coulombic

dx.doi.org/10.1021/nl302819f | *Nano Lett.* 2012, 12, 5664−5668

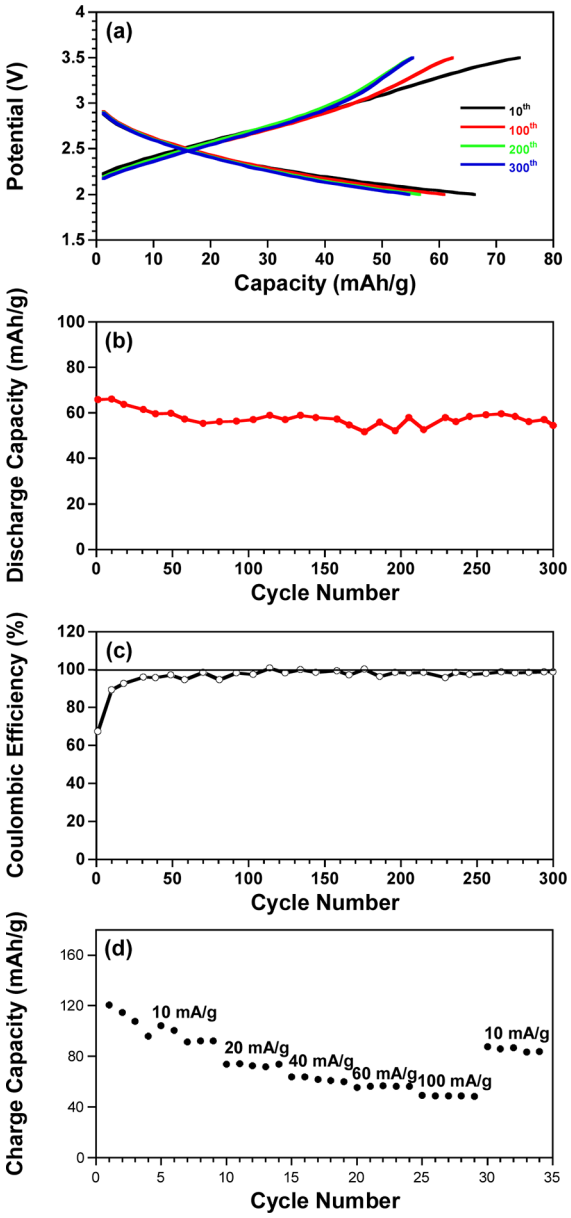

Figure 4. (a) Charge/discharge profiles in the 10th, 100th, 200th, and 300th cycles, (b) cycling stability at 50 mA/g, (c) Coulombic efficiency, and (d) rate capability of sodium-ion cells with $FePO_4$-SWNTs as the cathode.

efficiency approaches 98% after 40 cycles (Figure 4c), indicating excellent cycling stability and reversibility.

Until now, such a long cycling lifetime has not been reported for cathode electrode materials in sodium-ion batteries.[6,16−18] For example, Nazar and co-workers investigated the intercalation of sodium ions in a set of olivine-based metal phosphates (such as $FePO_4$, $NaMn_{0.5}Fe_{0.5}PO_4$, $NaMn_{0.8}Ca_{0.2}PO_4$, $NaMn_{0.8}Mg_{0.2}PO_4$, and Na_2FePO_4F).[4,20,21] However, no cycling performance was presented. The electrochemical and intercalated phase properties of $FePO_4$, $NaFePO_4$, $NaFePO_4F$, $Na_3V_2(PO_4)_3F_3$, $NaV_{1-x}Cr_xPO_4F$, and some other compounds were also studied by other groups either without cycling behaviors or limited cycle numbers.[6,10,18,22−28] In addition to phosphate crystal materials, layered metal oxide ($Na_4Mn_9O_{18}$, $Na_{0.44}CrO_2$, $NaNi_{0.5}Mn_{0.5}O_2$, and $Na_{2/3}Fe_{1/2}Mn_{1/2}O_2$) materials[16,29−33] have been reported as cathodes for Na-ion batteries but have also exhibited poor stability.

The results show that the amorphous $FePO_4$/SWNT composite is a promising cathode material for viable sodium-ion batteries. First, unlike the crystal-insertion reaction in which the structure phase changes upon ion insertion/extraction, the Na-ion insertion/extraction reaction does not change the structure of the amorphous $FePO_4$ materials, improving cycling stability.[8,14,15] Second, the large surface area of the porous $FePO_4$ ensures a high electrode−electrolyte contact area, which could significantly improve the charge transfer reaction for sodium ions and thus its kinetic property.[8,15]

Due to the poor electrochemical performance of electrode materials in sodium-ion batteries, the rate capability of electrodes for Na-ion battery has seldom been reported previously.[16−19] Here, the rate behaviors of the $FePO_4$/SWNTs composite were investigated at increased currents, shown in Figure 4d. The discharge capacity of as high as 120 mAh/g was delivered at a 0.1 C rate (10 mA/g), which is higher than most reported values of cathode materials for Na-ion cells. The capacity retentions are about 70 mAh/g, 60 mAh/g, and 55 mAh/g at higher currents of 20 mA/g, 40 mA/g, and 60 mA/g, respectively. Even at a 1 C rate (100 mA/g), a capacity of about 50 mAh/g was still retained. The high capacity retention at increased current clearly indicates high rate capability of the porous amorphous $FePO_4$/SWNTs composite. The improved electrochemical properties are believed to be associated with the unique structure of the composite. The carbon nanotube network and the porous structure provide good and fast transportation of electrons and sodium ions and facilitate the exchange of electrons and sodium ions at the $FePO_4$/electrolyte interface.

Cyclic voltammetry tests both on the complex of the $FePO_4$ nanoparticles and SWNTs and on pure SWNTs have also been performed, and the data are shown in Figure S6 in the Supporting Information. The electrochemical performance is different for materials with crystalline and amorphous structures. Typically, amorphous materials exhibit slope charge/discharge profiles, while crystal materials present flat plateaus. In the current case of the complex of amorphous $FePO_4$ nanoparticles and SWNTs, a slope feature was observed. But the curve observed (shown as black curves in Figure S6) is distinctively different from those of capacitors, since for capacitors, rectangular cyclic voltammetry curves are typical profiles. However, the CV curves observed from our materials (shown as black curves in Figure S6) clearly show redox peaks including a reduction peak at 1.8 V and an oxidation peak at 2.25 V, which are typical features for rechargeable batteries. On the contrary, a CV curve was collected for pure SWNTs (shown as red curves in Figure S6), and does not show any redox peaks. This observation once again confirms the redox reactions between Na and $FePO_4$.

In conclusion, a new type nanocomposite as a cathode material of SIBs has been produced following a one-step, facile hydrothermal process. The nanocomposite comprises of amorphous, porous $FePO_4$ nanoparticles connected by single-wall carbon nanotubes (SWNTs). While the porous $FePO_4$ nanostructures provide fast pathways for sodium ion transportation, SWNTs facilitate electron transportation. Consequently, the nanocomposite demonstrates an excellent cell performance with discharge capacities of as high as 66 mAh/g, along with a superior reversibility and stability for at least 300 cycles. Our current efforts are to extend this synthetic protocol

dx.doi.org/10.1021/nl302819f | Nano Lett. 2012, 12, 5664−5668

to other commercially available, low cost carbon-based materials, such as graphene, for better commercialization.

Experimental Section. *Materials.* Iron(II) ammonium sulfate hexahydrate ($(NH_4)_2Fe(SO_4)_2{\cdot}6H_2O$, 99%), phosphoric acid (H_3PO_4, 49−51%), urea (NH_2CONH_2), and sodium dodecylsulfate (SDS, ≥ 99.0%) were purchased from Aldrich, while the single-wall carbon nanotubes (−COOH or −OH functionalized) were purchased from SkySpring Nanomaterials, Inc. All chemicals and reagents were used as received.

Characterization. Samples for transmission electron microscopy (TEM) characterization were prepared by placing several drops of nanocrystal solutions in chloroform onto 300-mesh copper or nickel grids with carbon support film (no. 01753 or no. 01800, Ted Pella). Samples for scanning electron microscopy (SEM) were prepared by adding a couple drops of nanocrystal solutions in chloroform onto silica wafers. All high-resolution TEM (HR-TEM) images were taken from JEOL 2100F field-emission and 2100 LaB6 TEMs at 200 kV, while SEM images were taken on a Hitachi SU-70 Schottky field emission gun scanning electron microscope. Scanning TEM (STEM) images and energy-dispersive X-ray spectroscopy (EDX) spectra were acquired on a JEOL 2100F field-emission TEM operated at 200 kV.

Electrochemical Measurements. The $FePO_4$/SWNT composite was mixed with carbon black and poly(vinylidene difluoride) (PVDF) binder to form a slurry at the weight ratio of 8:1:1. The electrode was prepared by casting the slurry onto aluminum foil using a doctor blade and then dried in a vacuum oven at 100 °C overnight. Na-ion batteries were assembled with sodium as the counter electrode, 1 M $NaClO_4$ in a mixture of ethylene carbonate/dimethyl carbonate (EC/DMC, 1:1 by volume) as the electrolyte, and Celgard3501 (Celgard, LLC Corp., USA) as the separator. Electrochemical performance was tested using Arbin battery test station (BT2000, Arbin Instruments, USA). The capacity was calculated on the basis of the mass of $FePO_4$.

■ ASSOCIATED CONTENT

Ⓢ Supporting Information

SEM and TEM images, $FePO_4$ surface area and pore size, XRD data, and cyclic voltammetry curves. This material is available free of charge via the Internet at http://pubs.acs.org.

■ AUTHOR INFORMATION

Corresponding Author

*E-mail address: binghu@umd.edu, cswang@umd.edu.

Author Contributions

§These authors contributed to this work equally.

Notes

The authors declare no competing financial interest.

■ ACKNOWLEDGMENTS

This work is supported by startup funds from the University of Maryland College Park. C.W. and Y.X. acknowledge the support of the Army Research Office under Contract No.: W911NF1110231 (Dr. Robert Mantz, Program Manager) and Ellen Williams Distinguished Postdoctoral Fellowship and technical support of the Maryland NanoCenter.

■ REFERENCES

(1) Ong, S. P.; Chevrier, V. L.; Hautier, G.; Jain, A.; Moore, C.; Kim, S.; Ma, X.; Ceder, G. *Energy Environ. Sci.* **2011**, *4*, 3680−3688.

(2) Kim, S.-W.; Seo, D.-H.; Ma, X.; Ceder, G.; Kang, K. *Adv. Energy Mater.* **2012**, *2*, 710−721.

(3) Palomares, V.; Serras, P.; Villaluenga, I.; Hueso, K. B.; Carretero-Gonzalez, J.; Rojo, T. *Energy Environ. Sci.* **2012**, *5*, 5884−5901.

(4) Lee, K.-T.; Ramesh, T. N.; Nan, F.; Botton, G.; Nazar, L. F. *Chem. Mater.* **2011**, *23*, 3593−3600.

(5) Burba, C. M.; Frech, R. *Spectrochim. Acta, Part A* **2006**, *65*, 44−50.

(6) Moreau, P.; Guyomard, D.; Gaubicher, J.; Boucher, F. *Chem. Mater.* **2010**, *22*, 4126−4128.

(7) Wizansky, A. R.; Rauch, P. E.; Disalvo, F. J. *J. Solid State Chem.* **1989**, *81*, 203−207.

(8) Yin, Y. J.; Hu, Y. J.; Wu, P.; Zhang, H.; Cai, C. X. *Chem. Commun.* **2012**, *48*, 2137−2139.

(9) Lee, Y. J.; Belcher, A. M. *J. Mater. Chem.* **2011**, *21*, 1033−1039.

(10) Zaghib, K.; Trottier, J.; Hovington, P.; Brochu, F.; Guerfi, A.; Mauger, A.; Julien, C. M. *J. Power Sources* **2011**, *196*, 9612−9617.

(11) Kim, H.; Kim, S. W.; Hong, J.; Lim, H. D.; Kim, H. S.; Yoo, J. K.; Kang, K. *J. Electrochem. Soc.* **2011**, *158*, A930−A935.

(12) Gerbaldi, C.; Meligrana, G.; Bodoardo, S.; Tuel, A.; Penazzi, N. *J. Power Sources* **2007**, *174*, 501−507.

(13) Zhu, Y. J.; Wang, C. S. *J. Phys. Chem. C* **2011**, *115*, 823−832.

(14) Okada, S.; Yamamoto, T.; Okazaki, Y.; Yamaki, J.; Tokunaga, M.; Nishida, T. *J. Power Sources* **2005**, *146*, 570−574.

(15) Kim, S. W.; Ryu, J.; Park, C. B.; Kang, K. *Chem. Commun.* **2010**, *46*, 7409−7411.

(16) Ma, X. H.; Chen, H. L.; Ceder, G. *J. Electrochem. Soc.* **2011**, *158*, A1307−A1312.

(17) Vidal-Abarca, C.; Lavela, P.; Tirado, J. L.; Chadwick, A. V.; Alfredsson, M.; Kelder, E. *J. Power Sources* **2012**, *197*, 314−318.

(18) Kawabe, Y.; Yabuuchi, N.; Kajiyama, M.; Fukuhara, N.; Inamasu, T.; Okuyama, R.; Nakai, I.; Komaba, S. *Electrochem. Commun.* **2011**, *13*, 1225−1228.

(19) Komaba, S.; Murata, W.; Ishikawa, T.; Yabuuchi, N.; Ozeki, T.; Nakayama, T.; Ogata, A.; Gotoh, K.; Fujiwara, K. *Adv. Funct. Mater.* **2011**, *21*, 3859−3867.

(20) Ellis, B. L.; Makahnouk, W. R. M.; Rowan-Weetaluktuk, W. N.; Ryan, D. H.; Nazar, L. F. *Chem. Mater.* **2010**, *22*, 1059−1070.

(21) Ellis, B.; Makahnouk, W. R. M.; Makimura, Y.; Toghill, K.; Nazar, L. F. *Nat. Mater.* **2007**, *6*, 749−753.

(22) Recham, N.; Chotard, J. N.; Dupont, L.; Djellab, K.; Armand, M.; Tarascon, J. M. *J. Electrochem. Soc.* **2009**, *156*, A993−A999.

(23) Barker, J.; Saidi, M. Y.; Swoyer, J. L. *Electrochem. Solid-State Lett.* **2003**, *6*, A1−A4.

(24) Zhuo, H.; Wang, X.; Tang, A.; Liu, Z.; Gamboa, S.; Sebastian, P. J. *J. Power Sources* **2006**, *160*, 698−703.

(25) West, K.; Zachau-Christiansen, B.; Jacobsen, T. *Solid-State Ionics* **1988**, *28−30*, 1128−1131.

(26) Doeff, M. M.; Ferry, Y.; Ma, Y.; Ding, L.; Dejonghe, L. C. *J. Electrochem. Soc.* **1997**, *144*, L20−L22.

(27) Doeff, M. M.; Peng, M. Y.; Ma, Y.; Dejonghe, L. C. *J. Electrochem. Soc.* **1994**, *141*, L145−L147.

(28) Bach, S.; Millet, M.; Periera-Ramos, J. P.; Sanchez, L.; Lavela, P.; Tirado, J. L. *Electrochem. Solid-State Lett.* **1999**, *2*, 545−546.

(29) Cao, Y. L.; Xiao, L. F.; Wang, W.; Choi, D. W.; Nie, Z. M.; Yu, J. G.; Saraf, L. V.; Yang, Z. G.; Liu, J. *Adv. Mater.* **2011**, *23*, 3155−3160.

(30) Whitacre, J. F.; Tevar, A.; Sharma, S. *Electrochem. Commun.* **2010**, *12*, 463−466.

(31) Sauvage, F.; Laffont, L.; Tarascon, J.-M.; Baudrin, E. *Inorg. Chem.* **2007**, *46*, 3289−3294.

(32) Komaba, S.; Yabuuchi, N.; Nakayama, T.; Ogata, A.; Ishikawa, T.; Nakai, I. *Inorg. Chem.* **2012**, *51*, 6211−6220.

(33) Yabuuchi, N.; Kajiyama, M.; Iwatate, J.; Nishikawa, H.; Hitomi, S.; Okuyama, R.; Usui, R.; Yamada, Y.; Komaba, S. *Nat. Mater.* **2012**, *11*, 512−517.